Table IX. Entropy of Activation (cal K^{-1} mol^{-1}) Corrections Applied to A_8 (s^{-1}) = $10^{15.8}$ for IsBz To Estimate an A Factor for 1MeIn

	$\Delta S^{\ddagger}_{corr}$
symmetry	$-R \ln 2 = -1.4$
internal rotation	
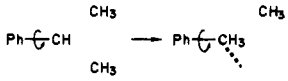	2.5
V (kcal mol^{-1}) = 2 → 12	
I (amu Å^2) ~ 56 → 17	
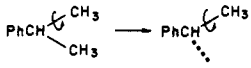	
V (kcal mol^{-1}) = 3.5 → 2.3	−0.2
total	0.9

It is informative to compare ΔRSE for DPhMe· and its radical analogue 10-hydro-9-anthryl (9AnH·). ΔRSEs of 4.5 kcal mol^{-1}

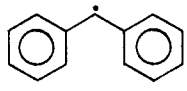

DPhMe·

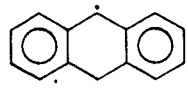

9AnH·

(present work) and 8 kcal mol^{-1},[1] respectively, have been determined experimentally. On the other hand, because DPhMe· and 9An· have the same formal π-structure their CSCs are the same, so SRT predicts that both radicals should have the same amount of extra resonance stability, 4.2 kcal mol^{-1}. Steric effects in DPhMe· may be the cause of its instability relative to 9AnH·. In DPhMe· one might expect interference between phenyl rings to not allow them to be coplanar, thereby diminishing conjugative stability. Such interference is not expected in 9AnH· which can easily assume a planar conformation. If this explanation is correct, steric effects (σ-bonds) would have to be explicitly taken into account in any general predictive method for RSE. The fact that eq 20 and 21 were scaled to fit the RSE for benzyl radical, which might contain steric energy due to repulsion between methylene and o-hydrogen atoms, may explain its accuracy for DPhMe· and related radicals. In any case, development of broader predictive models requires additional data as well as further theoretical analysis.

Summary

Differences in rates of benzyl C–CH_3 homolysis for reactions 2–6 and 7–9 were used to derive differences in resonance stabilities (RSE) of the benzylic radical products of these reactions. Structure Resonance Theory gave values of RSE in good agreement with our experimental results; however, a significant difference is found between our experimental RSE for DPhMe· and that reported in the literature for the related 10-hydro-9-anthryl radical, despite the fact that SRT predicts that they should have the same values. This difference, along with the result that SRT calculations work for DPhMe·, suggests that steric effects are inherently included in the existing parameters used in SRT calculations. Product mass spectra indicate that reactions 2–6 and 7–9 decompose solely by way of benzyl C–CH_3 homolysis. These results are not consistent with studies of Troe and co-workers of ethylbenzene decomposition where benzyl C–H homolysis was reported to be faster than benzyl C–CH_3 homolysis.

Appendix A

See Table VIII for a comparison of $\Delta S^{\ddagger}$ for 1PhBu and EtBz at 1076 K.

Appendix B

See Table IX for the entropy of activation corrections applied to A_8/s = $10^{19.8}$ for IsBz to estimate an A factor for 1MeIn.

Registry No. 4-EtSt, 3454-07-7; 1-PhBu, 824-90-8; 22-DPhPr, 778-22-3; Ph_2CHCH_3, 612-00-0; 1-MeIn, 767-59-9; 4-VyBz, 55185-65-4; 3-PhAl·, 20671-30-1; $MePh_2C$·, 51314-23-9; Ph_2CH·, 4471-17-4; In·, 79317-94-5.

Supplementary Material Available: Tables of VLPP rate constants, results of flow rate studies, and RRKM models (8 pages). Ordering information is given on any current masthead page.

(17) Stull, D. R.; Westrum, E. F.; Sinke, G. C. *The Chemical Thermodynamics of Organic Compounds*; Wiley: New York, 1969.
(18) Benson, S. W.; Cruickshank, F. R.; Golden, D. M.; Haugen, G. R.; O'Neal, H. E.; Rogers, A. S.; Shaw, R.; Walsh, R. *Chem. Rev.* **1969**, *69*, 279.
(19) Stein, S. E. *ThermoChim. Acta* **1981**, *44*, 265.

Vaporization of $(SN)_x$: He I Photoelectron Spectrum and ab Initio Calculations for the S_3N_3 Radical

W. M. Lau,[†] N. P. C. Westwood,*[‡] and M. H. Palmer[⊥]

Contribution from Guelph-Waterloo Centre for Graduate Work in Chemistry, Department of Chemistry and Biochemistry, University of Guelph, Guelph, Ontario, Canada N1G 2W1, Surface Science Western, Natural Science Centre, University of Western Ontario, London, Ontario, Canada N6A 5B7, and the Department of Chemistry, University of Edinburgh, West Mains Road, Edinburgh, Scotland, United Kingdom EH9 3JJ. *Received July 24, 1985*

Abstract: The S_3N_3 radical, never previously characterized, is shown to be the major semistable component of the vaporization products of the $(SN)_x$ polymer, as identified by He I photoelectron spectroscopy and in situ quadrupole mass spectrometry. This species can be recondensed to yield the $(SN)_x$ polymer and other colored materials. Revaporization produces S_3N_3 in addition to S_4N_4, S_4N_2, and S_2N_2. Ab initio calculations with better than a double-ζ basis set and including configuration interaction provide evidence for a $^2A_2$ radical with a planar ring geometry close to D_{3h}. The ground-state cation also has a planar ring geometry with $^3A_2'$ favored over $^1A_1'$.

The unusual $(SN)_x$ polymer with its highly anisotropic three-dimensional semimetallic properties, and low temperature superconductivity, has been the subject of considerable interest in recent years,[1] particularly since it can be incorporated into devices,[2] and offers prospects for the emerging molecular electronics.[3] The conventional production[4] of this polymer involves preparation and

† London.
‡ Guelph.
⊥ Edinburgh.

(1) Labes, M. M.; Love, P.; Nichols, L. F. *Chem. Rev.* **1979**, *79*, 1–15.
(2) Scranton, R. A. *J. Appl. Phys.* **1977**, *48*, 3838–3842.
(3) Munn, R. W. *Chem. Br.* **1984**, 518–524.

0002-7863/86/1508-3229$01.50/0 © 1986 American Chemical Society

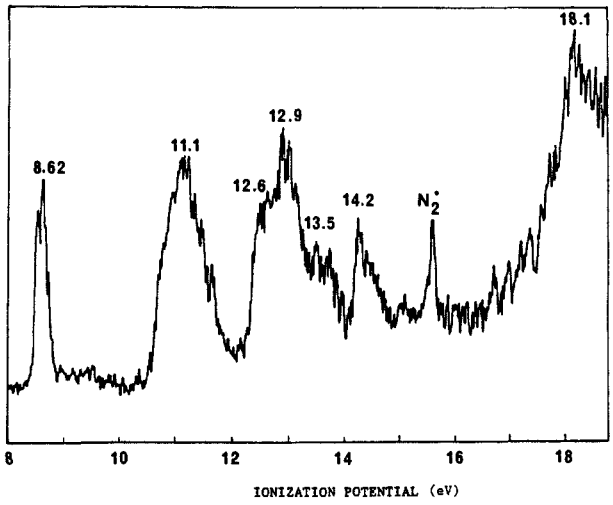

Figure 1. The He I photoelectron (PE) spectrum of the vaporization products of $(SN)_x$ at 140 °C. Numbers refer to ionization potentials at the band maxima, or estimated shoulders.

polymerization of the diamagnetic S_2N_2 molecule, a reaction which also has undergone intense scrutiny, both experimentally[1,5-7] and theoretically,[1,8-12] Previously,[13,14] we have investigated S_2N_2 using photoelectron spectroscopy and ab initio methods with a view to providing information on the electronic structure relevant to formation of the $(SN)_x$ polymer. In this work we address ourselves to $(SN)_x$ and its unpolymer-like property of vaporization and condensation back to $(SN)_x$,[1] which has provoked studies of the gas-phase intermediate(s) by mass spectrometric methods.[15-18] The essence of those conclusions is that a "linear bent" $(SN)_4$ unit (as distinct from the cradlelike S_4N_4 molecule) comprises ~85% of the gas-phase species.

Here we report a photoelectron/photoionization mass spectrometric study of the vaporization of the $(SN)_x$ polymer where the evidence supports the formation of an $(SN)_3$ radical species in the gas phase.[19] The *same* species is produced in the gas-phase pyrolysis of S_4N_4 over glass wool and is also present in the formation of S_2N_2 from pyrolysis of S_4N_4 over silver wool, albeit in lower yield. Ab initio CI calculations lend support to the identity of the $(SN)_3$ species, permit an evaluation of the structures of the ground-state radical and cation, and provide an analysis of the photoelectron (PE) spectrum.

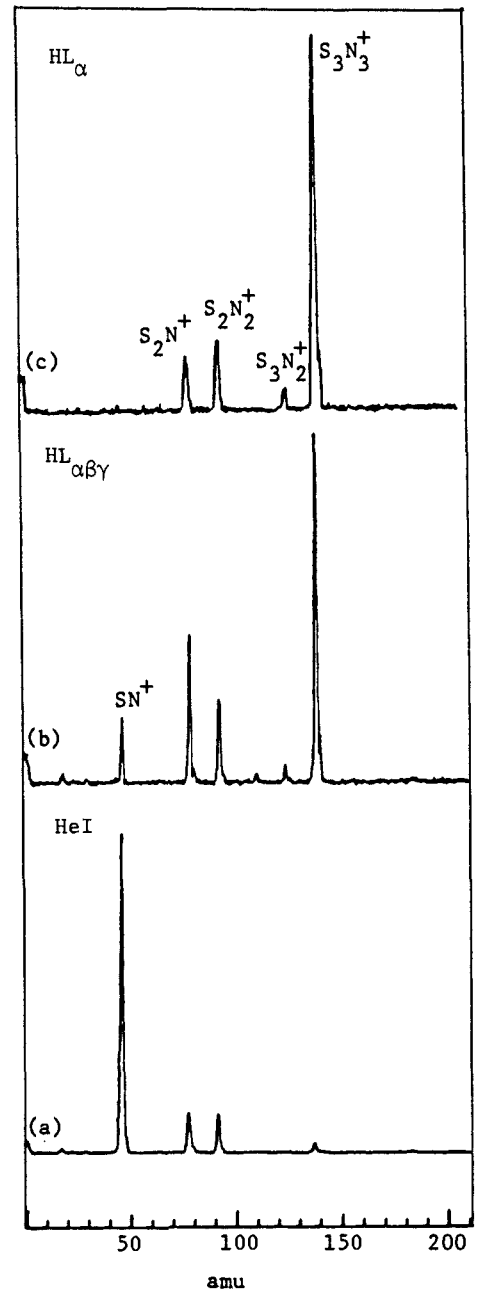

Figure 2. Photoionization mass spectra (PIMS) of the species in Figure 1 at different light source energies: (a) He I, 21.2 eV; (b) $HL_{\alpha,\beta,\gamma}$, 10.2–13.6 eV; (c) HL_α (filtered with LiF), 10.2 eV.

Experimental Section

The bulk of the $(SN)_x$ polymer was kindly provided by Dr. Richard Oakley (Department of Chemistry and Biochemistry, University of Guelph, Ontario). Other sources included IBM (San Jose) and samples that we prepared ourselves via polymerization of S_2N_2 (prepared by heating S_4N_4 over Ag wool).[5] $(SN)_x$ samples were placed in 10 mm o.d. Pyrex tubes attached directly to the ionization chamber of a fast-pumped photoelectron spectrometer specifically designed to study reactive and unstable species. This spectrometer, a modification of an earlier version,[20] permits not only measurement of the electron kinetic energies, but it can also mass analyze the ions produced in the photoionization process. This is achieved with a quadrupole mass analyzer (EAI 150, modified to reach 300 amu) mounted directly above the photoionization point. Although not done in coincidence, PE or photoionization mass spectra (PIMS) can be recorded within seconds of each other, thereby providing specific

(4) Recently, other methods have been devised; see, e.g.: Kennett, F. A.; MacLean, G. K.; Passmore, J.; Sudheendra Rao, M. N. *J. Chem. Soc. Dalton Trans.* **1982**, 851–857. Witt, M. W. R.; Bailey, W. I.; Lagow, R. J. *J. Am. Chem. Soc.* **1983**, *105*, 1668–1669.
(5) Mikulski, C. M.; Russo, P. J.; Saran, M. S.; MacDiarmid, A. G.; Garito, A. F.; Heeger, A. J. *J. Am. Chem. Soc.* **1975**, *97*, 6358–6363.
(6) Cohen, M. J.; Garito, A. F.; Heeger, A. J.; MacDiarmid, A. G.; Mikulski, C. M.; Saran, M. S.; Kleppinger, J. *J. Am. Chem. Soc.* **1976**, *98*, 3844–3848.
(7) Love, P.; Myer, G.; Kao, H. I.; Labes, M. M.; Junker, W. R.; Elbaum, C. *Ann. N.Y. Acad. Sci.* **1978**, *313*, 745–757.
(8) Kertesz, M.; Suhai, S.; Azman, A.; Kocjan, D.; Kiss, A. I. *Chem. Phys. Lett.* **1976**, *44*, 53–57.
(9) Baughman, R. H.; Chance, R. R.; Cohen, M. J. *J. Chem. Phys.* **1976**, *64*, 1869–1876.
(10) Salahub, D. R.; Messmer, R. P. *J. Chem. Phys.* **1976**, *64*, 2039–2047.
(11) Salahub, D. R.; Messmer, R. P. *Phys. Rev. B* **1976**, *14*, 2592–2602.
(12) Yamabe, T.; Tanaka, K.; Fukui, K.; Kato, H. *J. Phys. Chem.* **1977**, *81*, 727–731.
(13) Frost, D. C.; LeGeyt, M. R.; Paddock, N. L.; Westwood, N. P. C. *J. Chem. Soc., Chem. Commun.* **1977**, 217–218.
(14) Findlay, R. H.; Palmer, M. H.; Downs, A. J.; Egdell, R. G.; Evans, R. *Inorg. Chem.* **1980**, *19*, 1307–1314.
(15) Smith, R. D.; Wyatt, J. R.; DeCorpo, J. J.; Saalfeld, F. E.; Moran, M. J.; MacDiarmid, A. G. *Chem. Phys. Lett.* **1976**, *41*, 362–364.
(16) Smith, R. D.; DeCorpo, J. J.; Wyatt, J. R.; Saalfeld, F. E. *Int. J. Mass Spectrom. Ion Phys.* **1976**, *21*, 411–414.
(17) Smith, R. D.; Wyatt, J. R.; DeCorpo, J. J.; Saalfeld, F. E.; Moran, M. J.; MacDiarmid, A. G. *J. Am. Chem. Soc.* **1977**, *99*, 1726–1730.
(18) Saalfeld, F. E.; DeCorpo, J. J.; Wyatt, J. R.; Mah, P. T.; Allen, W. N. *Ann. N.Y. Acad. Sci.* **1978**, *313*, 759–766.
(19) For a preliminary account, see: Lau, W. M.; Westwood, N. P. C; Palmer, M. H. *J. Chem. Soc., Chem. Commun.* **1985**, 752–753.
(20) Frost, D. C.; Lee, S. T.; McDowell, C. A.; Westwood, N. P. C. *J. Electron. Spectrosc. Rel. Phenom.* **1977**, *12*, 95–109.

Table I. Vertical IP's for S and S–N Containing Molecules

molecule	IP's (eV)	ref
S_2	9.41, 11.82, 12.33, 13.20, 14.62, 15.58	56
S_2	9.53, 11.88, 12.33, 13.23	57
S_8	9.23, 9.47, 9.83, 10.12, 11.35, 12.54, 13.47, 14.08	58
SN	8.87	47
S_2N_2	10.52, 10.86, 10.05, 12.3, 14.40, 16.77	13
S_2N_2	10.51, 10.81, 11.06, 12.28, 14.42, 16.77	14
S_4N_4	9.36, 10.11, 10.60, 10.92, 11.44, 12.74, 13.66, 15.27	14
S_4N_2	8.58, 9.38, 10.72, 11.06, 12.10, 12.50, 13.23, 14.49	21

identification for unknown molecules (see, e.g., ref 21 and 22).

PE spectra were recorded for the known SN compounds, S_2N_2,[13,14] S_4N_4,[14] and S_4N_2,[21] together with the corresponding PIMS since we have found these molecules to be common products in the pyrolyses of SN compounds. In all cases, using the He I light source (21.2 eV) we were able to observe strong parent ion peaks in the mass spectra together with the typical fragmentation patterns. An advantage of this method is the ability to reduce the light source energy to, e.g., HL_α, 10.2 eV (filtered by LiF), and dramatically reduce the fragmentation.

Results

When the $(SN)_x$ polymer is heated (130–150 °C) in a commercial (Perkin-Elmer PS18) spectrometer, the PE spectrum is primarily S_2N_2 with traces of S_4N_4 and S_4N_2. Our instrument reproduces this at low pumping speeds, but when the analyzer pressure is reduced to 3×10^{-6} Torr by fast pumping the sample, the spectrum of Figure 1 is obtained. The poor S/N arises directly from the low vapor concentration where it is difficult to accumulate spectra over prolonged periods. IP values are shown on the figure and refer to peak maxima and estimated shoulder maxima. The corresponding PIMS is shown in Figure 2, using He I (21.2 eV), $HL_{\alpha,\beta,\gamma}$ (10.2–13.6 eV), and filtered HL_α (10.2 eV), and shows a highest mass peak at 138 amu (equivalent to $(SN)_3^+$), together with some fragmentation. No evidence for masses greater than 138 amu was obtained even at high sensitivity.

The PE spectrum in Figure 1 is assignable to essentially one molecular species (apart from traces of N_2) and is entirely reproducible. Interestingly, the same material can be observed in low concentration following pyrolysis of S_4N_4 over Ag wool during the synthesis of S_2N_2 and in somewhat greater yield in the pyrolysis of S_4N_4 over glass wool at 275 °C, together with S_2N_2, S_4N_4, and S_4N_2. The vaporization of $(SN)_x$ is, however, by far the most efficient route to this material. We note that at temperatures >150 °C the rate of vaporization is too high and the sample becomes rapidly depleted.

Identification

Previous evidence[15–18] has indicated that vaporization of $(SN)_x$ gives an open-chain $(SN)_4$ unit, which, if we are looking at the same species, is at variance with our results. The original evidence,[15–18] all from the same laboratory, involving 25 eV, 14 eV electron impact (EI), appearance potential (AP) measurements, field ionization (FI), and field desorption (FD) mass spectrometry, is not entirely convincing. For both FI and FD experiments peaks attributable to S_8^+ were observed which indicates decomposition, and in the EI experiments orange crystals indicative of S_4N_4 were observed around the orifice of the sampling region. We have demonstrated to our own satisfaction that under slower pumping conditions traces of S_2N_2, S_4N_4, and S_4N_2 can all be present. Additionally, we observe that vaporization and condensation can reform the $(SN)_x$ polymer; subsequent revaporization then leads to the formation of mass peaks *above* 138 amu, including 156 (S_4N_2) and 184 (S_4N_4). This is shown in Figure 3, and perhaps explains why, in several other instances when $(SN)_x$ was vaporized or revaporized,[23–25] such species appear in the mass spectra and

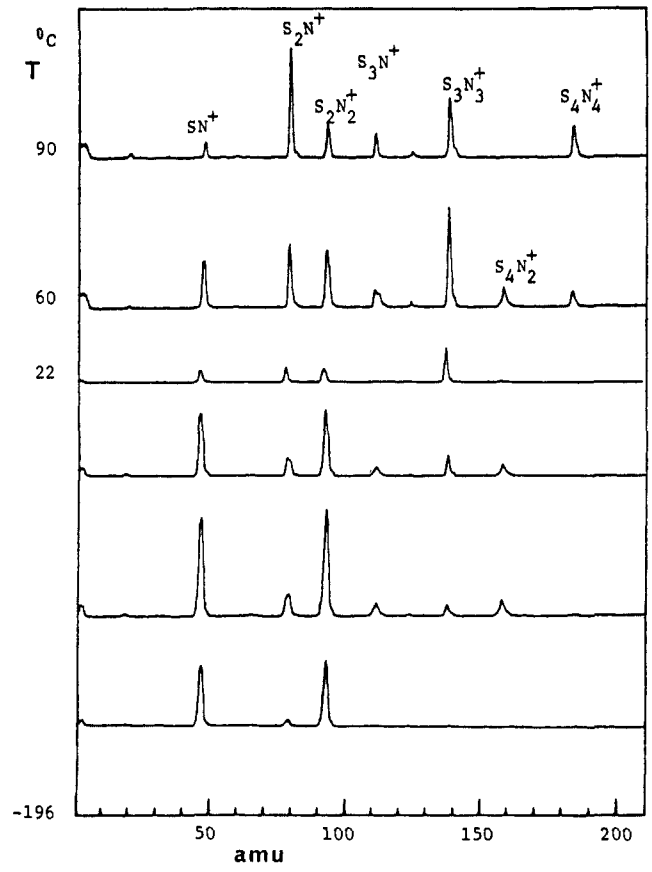

Figure 3. $HL_{\alpha,\beta,\gamma}$ photoionization mass spectra recorded following condensation (−196 °C) and vaporization of the species shown in Figures 1 and 2.

can lead to confusion regarding the precise nature of the vapor phase species. We note also that vaporized $(SN)_x$ when matrix isolated shows S_4N_4 and S_2N_2.[26,27]

The reported[15,17] AP's for S_2N_2 and S_4N_4 are ~1.1 eV too high when compared to the PE results for these molecules.[13,14] Table I assembles the IP's of S_2, S_8, SN, S_2N_2, S_4N_4, and S_4N_2 as obtained from photoelectron spectroscopy. This means that the AP observed[15,17] for $S_3N_3^+$ (9.5 eV) obtained from $(SN)_x$ under similar conditions is probably too high and could be as low as 8.4 eV, close to the IP of the species in Figure 1. This implies that $S_3N_3^+$ (138 amu) arises from direct ionization rather than fragmentation.

The phase angle mass spectrometric results[15,17] can be ascribed to an $(SN)_3$ parent neutral if the $(SN)_x$ were not in equilibrium, or if thermal relaxation had occurred. More likely, however, is that the $(SN)_3$ fragment results from S_4N_4 which, as we have noted above, can occur in the vaporization process.

In addition to these discrepancies the results of our experiments favor the identification of the vapor-phase species to $(SN)_3$ for several reasons.

(i) Our lowest ionizing energy (10.2 eV) is well below that used for EI and therefore minimises fragmentation, with no evidence for peaks above 138 amu in the mass spectrum. Indeed, with filtered HL_α, an intense $S_3N_3^+$ peak is observed and most noticeably there is *no* SN^+ fragment.

(ii) The He I photoelectron spectrum shows a sharp first band with a separation of ~2.5 eV to the next ionization potential (IP). Such a distinct first band is very unusual for a molecule containing

(21) Palmer, M. H.; Lau, W. M.; Westwood, N. P. C. *Z. Naturforsch.* **1982**, *37a*, 1061–1067.
(22) Frost, D. C.; Lau, W. M.; McDowell, C. A.; Westwood, N. P. C. *J. Phys. Chem.* **1982**, *86*, 3577–3581.
(23) Cavanagh, R. R.; Altman, R. S.; Herschbach, D. R.; Klemperer, W. *J. Am. Chem. Soc.* **1979**, *101*, 4734–4735.
(24) Kelemen, S. R.; Herschbach, D. R. *J. Phys. Chem.* **1982**, *86*, 4388–4392.
(25) Kennett, F. A.; MacLean, G. K.; Passmore, J.; Sudheendra Rao, M. N. *J. Chem. Soc., Dalton Trans.* **1982**, 851–857.
(26) Teichman, R. A.; Nixon, E. R. *Inorg. Chem.* **1976**, *15*, 1993–1994.
(27) Iqbal, Z.; Downs, D. S. *Chem. Phys.* **1979**, *44*, 137–142.

at least three sulfur and three nitrogen atoms. Thus, for example, within 2.5 eV of the first IP, the He I PE spectrum of S_2N_2[13,14] shows three resolved bands, that of S_4N_2[21] shows four bands, and that of S_4N_4[14] shows six bands. A linear $(SN)_4$ biradical or a cyclic $(SN)_4$ molecule would give a more complex ionization pattern; compare, e.g., the SCF–X_α–SW calculations on an open-chain $(SN)_4$ model[11] which shows ionization processes from 2 σ and 1 π orbitals within the first 1.7 eV (see also ref 12). In fact, computed IP's for a complete selection of "linear" $(SN)_y$ (y = 2–6) species[28] indicate several bands below 10 eV in all cases.

(iii) In a recent paper[29] the possible observation of S_3N_3 has been claimed, following pyrolysis of S_4N_4 over glass or silver wool. It was stated that the $(SN)_4$ isomer is not found by this route. In identical PE/PIMS experiments involving pyrolysis of S_4N_4 over glass/silver wool we see *exactly the same* species as observed in the vaporization of $(SN)_x$. Whereas the polymer route yields virtually 100% S_3N_3, the S_4N_4 pyrolyses give less yields and, in addition, show the presence of S_2N_2, S_4N_4, and S_4N_2. We also note that thermal decomposition of S_4N_4 has been used as a route to $(SN)_x$,[30] entirely consistent with our observations involving the intermediacy of S_3N_3.

(iv) Once formed the vapor species can travel more than 25 cm in an 8 mm i.d. glass tube with only very minor decomposition; most of it still survives after passage through Pyrex wool at 300 °C. Above 450 °C, S_2, N_2, and S_2N_2 are produced. Although speculative the implication is that there is some additional stability imparted to S_3N_3 by, say, ring formation, compared to a biradical linear $(SN)_4$ species. At distances much greater than 25 cm, S_2N_2, S_4N_2, and S_4N_4 begin to appear.

(v) Although the species in question is relatively stable in the vapor phase it undergoes substantial changes upon condensation at −196 °C. A film gradually develops with hues of red, brown, white, and blue; the red portion is the most volatile. Such colors have been noted previously as precursors to the $(SN)_x$ preparation, including evidence for a red paramagnetic species.[7] Upon warming back to room temperature, S_2N_2, S_3N_3, and S_4N_2 emerge from this condensate, and a dark blue film characteristic of the polymer develops. Warming this film gives S_2N_2, S_3N_3, S_4N_2, and S_4N_4. Thus the species can be trapped and revaporized although with some decomposition.

In short we believe that the dominant species produced in the gas-phase vaporization of $(SN)_x$ is S_3N_3, which under certain conditions, e.g., trapping and revaporizing, or after many wall collisions can produce quantities of S_2N_2, S_4N_2, and S_4N_4 thereby leading to possible confusion in earlier mass spectrometric studies. It is only in the very direct sampling used here that we can produce virtually 100% S_3N_3°.

Since S_3N_3° and $S_3N_3^+$ are essentially unknown species, although often the subject of some speculation,[29,31-34] we assess in the next section the possibility of a cyclic structure akin to that of the S_3N_3 anion[34] before embarking the extensive (and expensive) electronic structure calculations.

Structure of the S_3N_3 Radical

There are several pieces of evidence that point toward a cyclic structure for S_3N_3°.

(1) As mentioned above, the pattern of the PE spectrum argues against a quasilinear structure.

(2) Vapor-pressure studies[17,35] show a small vaporization coefficient ($\sim 3 \times 10^{-3}$) and the magnitude of the heat of vaporization is ~30 kcal mol^{-1} compared to ~50–60 kcal mol^{-1} for the S–N bond. This is strongly suggestive of ring formation.

(3) A molecular beam electric deflection analysis[23] of the $(SN)_x$ vapors noted that S_8^+, $S_4N_4^+$, $S_4N_2^+$, and $S_3N_3^+$ were all detected, the latter mass peak being defocused by the electric field indicating a nonpolar neutral precursor. This is good evidence for a ring structure. Interestingly, the defocused $S_4N_4^+$ peak indicates a nonpolar structure for this neutral precursor also, evidence against a linear $(SN)_4$ species and supporting our contention that this is actually the cradle version of S_4N_4.

(4) The S_3N_3 anion[34] has been shown to be a planar ring, and chemical intuition suggests that the S_3N_3 radical would also be a ring; one-electron oxidation of $S_3N_3^-$ to S_3N_3° should strengthen the π framework of the cyclic structure.[32] The S_3N_3 cation energy levels have been calculated assuming a D_{3h} ring structure;[34] the calculated separation between the LUMO (lowest unoccupied MO) and the HOMO (highest occupied MO) of the cation is 3.38 eV. This separation can be correlated with the difference between the first and second IP's of the corresponding neutral, when allowance is made for the differences between adiabatic and vertical IP's and triplet/singlet splittings. The relatively large experimental gap of 2.5 eV thus agrees fairly well with this crude estimate and provides some support for a ring S_3N_3 structure. We note also, from the vertical nature of the ionization process leading to the ground-state cation (Figure 1), that the neutral radical must have a similar geometry.

(5) Although not strong evidence, we mention that a minimal basis calculation on an $(SN)_3$ trimer found it to be more stable than two dimers.[36] A ring trimer structure was not attempted, but interestingly, a square-planar S_2N_2 molecule was found to be more stable than the chain $(SN)_2$ structure.

Given the above evidence for a cyclic structure for S_3N_3° and the planar D_{3h} structure of the known 10 π $S_3N_3^-$ system,[32,34,37-40] it seemed reasonable to use similar structures for the radical and cations with 9 and 8 π electrons, respectively. However, it is feasible that the latter pair may not be planar and singlet vs. triplet possibilities can occur with the cations. In order to provide a point of reference with previous work,[34,40] we have also performed calculations on the anion, $S_3N_3^-$, at the crystal structure **1**.

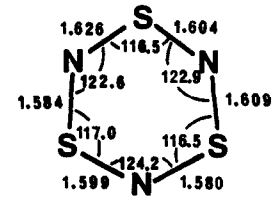

[1]

Computational Methods

(i) **Basis Sets.** Geometry optimization was carried out with a minimal S/N atomic orbital basis (MB) consisting of (11s6p1d/7s3p) contracted to [3s2p1d/2s1p] as in our previous optimization of S_4N_2.[41] The main SCF/CI studies were continued at the computed equilibrium geometries of the various states (below) by using an S/N double-ζ (DZ) basis (13s9p1d/9s5p) contracted to (7s4p1d/4s2p) as in our earlier work;[21,42] it is thus slightly larger than DZ in s functions.

(ii) **Geometry Optimization.** Our previous work (compare ref 41) used HONDO-6 which proved incapable of handling e^2 and

(28) Palmer, M. H., unpublished results. See also: Palmer, M. H.; Findlay, R. H. *J. Mol. Struct. (THEOCHEM)* **1983**, *92*, 373–383.
(29) Smith, R. D. *J. Chem. Soc., Dalton Trans.* **1979**, 478–481.
(30) Louis, E. J.; MacDiarmid, A. G.; Garito, A. F.; Heeger, A. J. *J. Chem. Soc., Chem. Commun.* **1976**, 426–427.
(31) Chivers, T.; Sudheendra Rao, M. N. *Can. J. Chem.* **1983**, *61*, 1957–1962.
(32) Chivers, T.; Cordes, A. W.; Oakley, R. T.; Pennington, W. T. *Inorg. Chem.* **1983**, *22*, 2429–2435.
(33) Zhu, J.-K.; Gimarc, B. M. *Inorg. Chem.* **1983**, *22*, 1996–1999.
(34) Bojes, J.; Chivers, T.; Laidlaw, W. G.; Trsic, M. *J. Am. Chem. Soc.* **1979**, *101*, 4517–4522. Laidlaw, W. G., private communication.
(35) Weber, D. C.; Ewing, C. T. *Inorg. Chem.* **1977**, *16*, 3025–3077.
(36) Deutsch, P. W.; Curtiss, L. A. *Chem. Phys. Lett.* **1977**, *51*, 125–131.
(37) Waluk, J. W.; Michl, J. *Inorg. Chem.* **1981**, *20*, 963–965.
(38) Chivers, T.; Laidlaw, W. G.; Oakley, R. T.; Trsic, M. *Inorg. Chim. Acta* **1981**, *53*, L189–L190.
(39) Smith, V. H.; Sabin, J. R.; Broclawik, E.; Mrozek, J. *Inorg. Chim. Acta* **1983**, *77*, L101–L104.
(40) Nguyen, M. T.; Ha, T.-K. *J. Mol. Struct. (THEOCHEM)* **1983**, *105*, 129–134.
(41) Palmer, M. H.; Wheeler, J. R.; Findlay, R. H.; Westwood, N. P. C.; Lau, W. M. *J. Mol. Struct. (THEOCHEM)* **1981**, *86*, 193–195.
(42) Redshaw, M.; Palmer, M. H.; Findlay, R. H. *Z. Naturforsch.* **1979**, *34a*, 220–232.

Table II. Energies of S_3N_3 Optimized Structures[a] (au)

structure	basis	state	molecule	energy	method (level)
C_{2v}					
2	MB	$^2A_2$	R	−1353.01167	SCF
4	MB	$^1A_1$	SC	−1352.74568	SCF
5	MB	$^3B_2$	TC	−1352.81122	SCF
2	DZ	$^2A_2$	R	−1355.6486	SCF
2	DZ	$^2A_2$	R	−1356.11530	CI (5)
4	DZ	$^1B_2$	SC	−1355.80462	CI (6)
4	DZ	$^1A_1$	SC	−1355.81144	CI (10)
4	DZ	$^1A_2$	SC	−1355.75534	CI (9)
4	DZ	$^1B_1$	SC	−1355.73105	CI (9)
5	DZ	$^3B_2$	TC	−1355.80950	CI (6)
5	DZ	$^3A_1$	TC	−1355.76055	CI (9)
5	DZ	$^3A_2$	TC	−1355.75350	CI (9)
5	DZ	$^3B_1$	TC	−1355.74774	CI (8)
D_{3h}					
6	MB	$^2E''$	R	−1353.03860	SCF
6	DZ	$^2E''$	R	−1355.68249	SCF
6	DZ	$^2A_2''$ ($^2A_2$)	R	−1355.69550	SCF
6	DZ	$^2A_1'$ ($^2A_1$)	R	−1356.02789	CI
6	DZ	$^2A_2''$ ($^2A_2$)	R	−1356.12650	CI
6	DZ	$^2E''$	R	−1356.11273	CI
6	DZ	$^3A_2'$ ($^3B_2$)	TC	−1355.41374	CI
6	DZ	$^1A_1'$ ($^1A_1$)	SC	−1355.37256	CI
6	DZ	$^1A_1'$ ($^1A_1$)	A	−1355.76104	CI

[a] R = radical, SC = singlet cation, TC = triplet cation, A = anion.

e^3 configurations in D_{3h} and also only performed UHF rather than RHF computations on the radical C_{2v} or C_s structures. Recent work has shown that minimal basis UHF structures, in contrast to the corresponding RHF ones, are often significantly different from experimental results.[43] Most of the optimization was carried out with GAMESS[44] implemented on the ULCC CRAY-1s. The final C_{2v} structures obtained are shown for the radical using UHF (**2**) and RHF wave functions (**3**), the singlet (**4**) and triplet (**5**) cations, and the corresponding D_{3h} structures **6**, **7**, and **8** (note, **7** and **8** give identical structures). The corresponding energies are given in Table II.

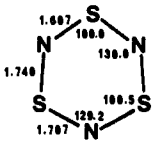

[2] C_{2v} radical UHF

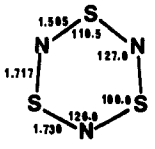

[3] C_{2v} radical RHF

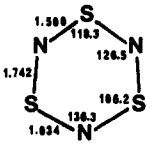

[4] C_{2v} singlet cation

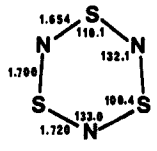

[5] C_{2v} triplet cation

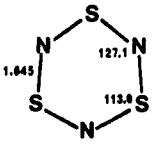

[6] D_{3h} radical

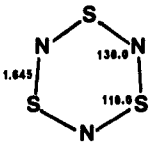

[7] D_{3h} singlet cation
[8] D_{3h} triplet cation

(iii) The DZ-CI Study. For each SCF wave function the method was identical; the core electrons and three innermost pairs ($2s_N$ largely) of the valence shell were frozen (Tables III and IV), yielding an active set of 27/26 electrons for $S_3N_3^\circ/S_3N_3^+$, respectively. All configurations generated by double replacements into the lowest 30 SCF virtual orbitals, in Aufbau order, were obtained by using the MRDCI program (see ref 45 for further details of the method); in practice this program recognizes only reflection planes, so that D_{3h} and C_{2v} proceed along similar lines. The relationship for $C_{2v} \rightarrow D_{3h}$ is $(a_1 + b_2) \rightarrow (a_1' + a_2' + e')$, $(b_1 + a_2) \rightarrow (a_2'' + e'' + a_1'')$. The multireference CI had (typically) 10 reference configurations and these were selected over more than one calculation, as the set which produced the first few CI roots of the required symmetry. In the first phase, the reference set was the Koopmans' set using occupied orbitals from $(2e'')^3$ down to $3a_1'$; these were then supplemented by shakeup reference configurations on an ad hoc basis till the required number of roots had been obtained. Experience showed that the LUMO ($2a_2''$) was critical to the shakeup manifold; this parallels the situation with S_2N_2.[45] As well as incorporating genuine shakeup $\pi^* \rightarrow \pi^*$ states, the effect of the CI on the SCF wave function is to refine the wave function by introduction of the second orbital ($2a_2''$) where only one orbital of that symmetry ($1a_2''$) is occupied in the ground state.

Computational Results

(i) At the SCF Level. (a) Geometry Optimization. As mentioned above the *n*-Bu_4N^+ salt of $S_3N_3^-$ (**1**) has a D_{3h} structure with SN ~1.60 Å, N ~123°, S ~117°.[34] Other ab initio geometry optimizations[40] for this species show the importance of d functions, since a DZ sp-basis led to SN 1.720 Å, whereas a smaller split valence basis augmented by $3d_s$ gave a better value at SN 1.641 Å. The angles were not reported. When a C_s symmetry radical was started from structure **2**, but with the axial S,N atoms tilted out of plane by + and −30° (chair form), the RHF calculation oscillated through both shallow boat and chair forms, finally converging on the planar (C_{2v}) structure **3**. The energy surface to bending is clearly relatively shallow, as expected. In all cases of the chair and boat forms, the unpaired electron was strongly located upon the C_s axis N atom, with the N=S=N unit being little changed.

The current results for each of the cations **4**, **5**, **7**, and **8** and the radicals **2**, **3**, and **6** show bond lengths and angles in the general range expected from the crystallographic anion study of **1**.[34] From the photoionization aspect, the change in geometry for the C_{2v} series radical **2** to triplet cation **5** is small, the angles changing by 4° or less and the bond lengths by 0.04 Å. The results for the D_{3h} series radical **6** to triplet cation **8** are similar, and both lie lower in energy than the C_{2v} series. This concords with the sharp first IP, i.e., little difference between adiabatic and vertical.

(b) The DZ Calculations. Although there is no direct comparison with earlier work for the S_3N_3 radical and cations, our SCF energy for $S_3N_3^-$, $^1A_1'$ **1** using the radical optimized D_{3h} structure **6** (Table II), is about 0.3 au lower than the previously reported[40] value and reflects the larger (105 CGTO's) spd basis. There are two closely spaced pairs of orbitals changed in relative positions ($3e'/1e''$ and $3a_1'/1a_2''$) compared to the earlier work;[34,40] the LUMO for the anion, $2a_2''$, a π^*-orbital, has the same symmetry as previously determined.[34,40]

For the S_3N_3 radical the DZ calculations confirmed the MB relative energy order of structures **2** and **6**, with the latter (D_{3h}) preferred by 0.027 au (MB), 0.034 au (DZ) (Table II). Curiously, the D_{3h} radical structure **6** yielded a 9π $^2A_2''$ state ($^2A_2$ in C_{2v}) at slightly lower energy than $^2E''$ (0.013 au, 0.35 eV), by appropriate "swapping" of electrons and reconvergence. This relative order was confirmed by the CI (0.0134 au, 0.37 eV). A feature of the $^2A_2''$ calculations is the wide separation of the now nondegenerate $(2e'')^3$ pair of orbitals $(3a_2'')^2$ and $(2a_1'')^1$ ($3b_1$ and $2a_2$ in C_{2v}, Table IV; Figure 4). The additional stabilization of $(2e'')^3$ is 1.6 eV relative to $(2a_1'')^1$, an important feature with respect to stability to oxidizing agents. In summary, the slightly lower energy of $^2A_2''$ relative to $^2E''$ for $S_3N_3^\circ$ points toward Jahn–Teller distortion in the molecule, but the experimental structure is probably closer to **6** than **2**.

The triplet cation **5** (C_{2v}) is lower in energy than the singlet cation **4** (C_{2v}) with a triplet–singlet splitting of 1.8 eV (MB), although C_{2v} DZ calculations give them as essentially equal. The DZ (D_{3h}) calculation reestablishes a lower triplet energy by 1.12 eV ($^1A_1'$–$^3A_2'$).

(ii) The CI Study. A number of SCF wave functions were tested in the first phase of the CI by using both C_{2v} and D_{3h} structures (**2** and **6**) to find which would give the best energy for $S_3N_3^\circ$ and

(43) Farnell, L.; Pople, J. A.; Radom, L. *J. Phys. Chem.* **1983**, *87*, 79–82.
(44) Provided by M. F. Guest, SERC, Daresbury Laboratory, U. K.
(45) Palmer, M. H. *Z. Naturforsch.* **1984**, *39a*, 102–108.

Table III. Sequence Numbers and Labels for Valence Shell Orbitals of S_3N_3

																		SOMO	LUMO		
SCF no.	19	20	21	22	23	24	25	26	27	28	29	30	31	32	33	34	35	36	37	38
CI no.	frozen			25	1	26	2	3	16	27	4	17	38	28	5	18	39	19	29	6
orbital (C_{2v})	$1a_1$	$1b_2$	$2a_1$	$2b_2$	$3a_1$	$3b_2$	$4a_1$	$5a_1$	$1b_1$	$4b_2$	$6a_1$	$2b_1$	$1a_2$	$5b_2$	$7a_1$	$3b_1$	$2a_2$	$4b_1$	$6b_2$	$8a_1$
orbital (D_{3h})	$1a_1'$	$1e'$		$2e'$		$1a_2'$	$2a_1'$	$3a_1'$	$1a_2''$	$3e'$		$1e''$		$4e'$		$2e''$		$2a_2''$	$5e'$	
									π			π				π		π		

Table IV. Double-ζ SCF Orbitals and Energies (eV) for $S_3N_3^{\circ}$ [a]

	Structure **2**, C_{2v}, $S_3N_3^{\circ}$, $^2A_2$
a_1	34.46, 32.46, 26.15 (1), 19.37 (2), 16.60 (3), 14.69 (4), 11.56 (5)
b_2	32.68, 26.48 (25), 19.32 (26), 14.59 (27), 12.47 (28)
b_1	16.20 (16), 13.77 (17), 8.23 (18)
a_2	13.38 (38), 5.49 (39)
	Structure **6**, D_{3h}, $S_3N_3^{\circ}$, $^2A_2''$
a_1	36.53, 33.38, 26.81 (1), 18.84 (2), 17.11 (3), 14.56 (4), 12.11 (5)
b_2	33.80, 26.76 (25), 20.57 (26), 14.87 (27), 12.59 (28)
b_1	16.95 (16), 14.06 (17), 8.43 (18)
a_2	14.16 (38), 5.26 (39)
	Structure **6**, D_{3h}, $S_3N_3^{\circ}$, $^2E''$
a_1'	36.51, 18.85 (2), 17.01 (3)
a_2'	20.26 (26)
e'	33.58, 26.78 (1, 25), 14.72 (4, 27), 12.35 (5, 28)
a_2''	16.96 (16)
e''	14.11 (17, 38), 6.85 (18, 39)

[a] CI sequence numbers in parentheses.

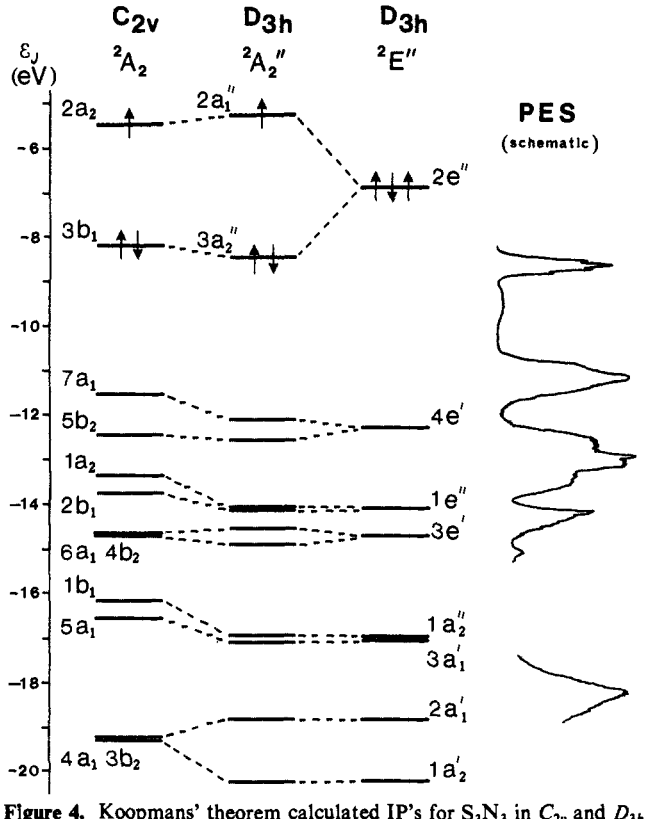

Figure 4. Koopmans' theorem calculated IP's for S_3N_3 in C_{2v} and D_{3h} (with $^2A_2''$ and $^2E''$ wave functions) and comparison with a schematic photoelectron spectrum.

triplet $S_3N_3^+$; all these studies were under comparable conditions and used the wave functions from the $^3A_2'$ ($^3B_2$) cation, $^2A_2''$ and $^2E''$ radical, and $^1A_1'$ anion. The best results were obtained from the $^2A_2''$ and $^2E''$ wave functions (both D_{3h}) and these were used for calculation of the PE spectrum.

Given the Hückel ($4n + 2$) π-electron rule for cyclic species where degenerate π levels occur, $S_3N_3^+$ and $S_3N_3^-$ have 8 and 10 π electrons, respectively and thus should be triplet and singlet states, respectively. The radical $S_3N_3^{\circ}$ can in principal be either $^2\Pi$ or $^2\Sigma$; the former 9 π and the latter 10 π. The present results

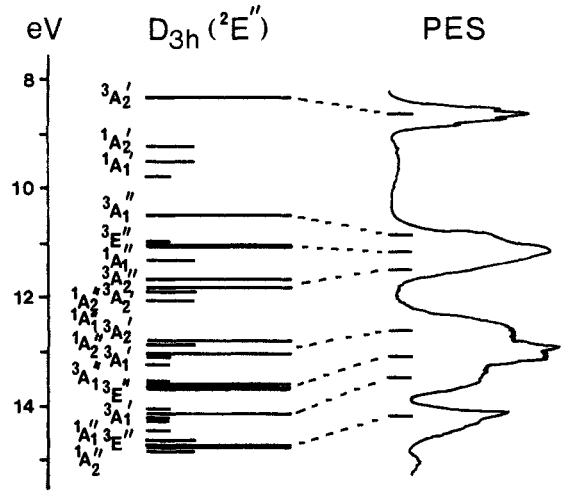

Figure 5. Calculated cationic states for S_3N_3 (D_{3h}, $^2E''$ wave function, SERHF) and comparison with experiment. Long and short lines refer to triplet and singlet states, respectively; very short lines (unlabeled) correspond to shakeup states (see Table V) of unknown intensity.

(Table II) show a preference of about 0.1 au (2.7 eV) for the $^2\Pi$ ($^2A_2''$ and $^2E''$) system over $^2\Sigma$ ($^2A_1'$).

Assignment of the UV Photoelectron Spectrum

The experimental spectrum (Figure 1) is characterized by 4 main groups of bands, centered at 8.6, 11.1, 12.9, and 14.2 eV, together with a weak band near 15 eV and more intense regions to higher binding energy. The present work is only concerned with the 8–15-eV region. The 11-eV group shows shoulders to both sides of the main peak, and 3 or more IP's seem likely; a similar situation occurs with the 13-eV band with more extensive structure.

The calculated energies of the cationic states from the $^2A_2''$ wave function in D_{3h} symmetry were slightly lower in energy in all cases relative to cations derived from the $^2E''$ wave function. However, the wide separation of the singly occupied MO (SOMO) $2a_1''$ and the $3a_2''$ (DOMO) made the interpretation of the UPS more complex; the same situation applies when the C_{2v} structure **2** is utilized ($2a_2$ and $3b_1$ orbitals). This is seen by the following example for $S_3N_3^{\circ}$ and by using Figure 4. The Koopmans' states with occupancy A(... $3b_1^2\,2a_2^1$) and B(... $3b_1^1\,2a_2^2$) are not degenerate, (compare C(... $(2e'')^3$); indeed B is a shakeup state of A. With the double open shell states of $S_3N_3^+$, the situation becomes more complex, and the distinction between Koopmans' states (expected to be relatively strong in the UPS) and shakeup states (weak) becomes confused. In practice neither of these proved acceptable interpretations of the PE spectrum, and so the finally adopted SCF wave function was $^2E''$ for the radical and the vertical IP's were computed from this; these symmetry equivalenced RHF (SERHF) results are shown in Table V and Figure 5. The numerical values for the CI states obtained with the $^2A_2$ wave functions (structures **2** and **6**) are also tabulated.

All the cationic triplet states down to about 15 eV were computed from the D_{3h} $^2E''$ wave function, and most of the singlet states as well. We shall assume that the relative intensities reflect the spin–orbit degeneracies, i.e., 3:1 for triplet/singlet, with shakeup peaks from either set being even less intense.

The principal results of the multireference CI (Table V) show that triplet states rich in each of the orbitals 4e' (C_{2v}, CI sequence

Table V. Energies of Triplet and Singlet $S_3N_3^+$ and IP's from the D_{3h} Structure

ex $^2A_2''$ Wave Function

state	energy (+1355 au)	IP (eV)[a]	open shells[b]				C_i^2	type[c]	state	energy (+1355 au)	IP (eV)[a]	open shells[b]				C_i^2	type[c]
$^3A_1$	−0.7588	9.80	18	19			0.7184	S	$^3B_2$	−0.8349	7.65	18	39			0.8311	K
	−0.6912	11.78	18	18	38	39	0.7813	S/K		−0.7457	10.04	19	39			0.6374	S
	−0.6704	12.82	38	39	17	18	0.6502	K/S		−0.6815	12.30	18	38			0.5637	S
	−0.5895	14.81	16	18			0.6564	K		−0.6449	14.07	17	39	18	38	0.5895	K/S
			18	19	38	39	+0.1280			−0.6301	14.11	4	28			0.7891	S
	−0.5543	16.43	18	19	38	39	0.7061	S				19	38			+0.1143	
$^3A_2$	−0.7651	9.85	18	28	5	39	0.7414	S/K	$^3B_1$	−0.7706	9.92	5	18	28	39	0.7408	S
	−0.7329	10.89	5	39	18	28	0.7624	K/S		−0.7469	10.66	5	18	28	39	0.6586	K
	−0.6450	13.47	18	27			0.7114	S		−0.6632	12.60	18	19	28	39	0.6847	S
										−0.6515	13.13	4	18			0.5686	S
												18	19	28	39	+0.2182	
										−0.6375	13.85	18	19	28	39	0.4669	S
												3	18			+0.1077	
												4	18			+0.1026	

ex $^2E''$ Wave Function

state	energy (+1355 au)	IP (eV)[a]	open shells[b]				C_i^2	type[c]	state	energy (+1355 au)	IP (eV)[a]	open shells[b]				C_i^2	type[c]
$^3A_1'$	−0.7404	10.94*	18	19			0.7127	S	$^1A_1'$	−0.8030	9.52	none[d]				0.8041	K
	−0.6738	13.03	38	39			0.4283	K		−0.7879	9.71	none[e]				0.8035	S
($^3A_1$)			17	18			0.2721		($^1A_1$)	−0.6615	13.70	18	19			0.5675	S
	−0.6474	14.17	38	39			0.1895	K				38	39			0.1176	
			17	18			0.4594			−0.6190	15.61	38	39			0.2857	S
	−0.6196	14.71#	16	18			0.5244	K				17	18			0.2222	K
			18	19	38	39	0.1462					18	19			0.1658	S
	−0.5725	16.02	18	19	38	39	0.6447	S									
	−0.5470	16.80	17	19			0.5507	S	$^1A_1''$	−0.7356	11.21	18	28			0.5187	K
												5	39			0.2642	K
$^3A_2'$	−0.8317	8.31	18	39			0.8466	K	($^1A_2$)	−0.7150	12.16	5	39			0.5225	K
	−0.7385	10.93*	19	39			0.7138	S				18	28			0.2646	K
($^3B_2$)	−0.7049	11.80	17	39	18	38	0.8206	K		−0.6234	14.65	4	39			0.6738	K
	−0.6943	12.78	17	39	18	38	0.6810	K		−0.6177	15.04	19	28			0.6425	S
	−0.6316	14.45	5	28			0.8082	S									
	−0.6222	14.77#	16	39			0.7042	K	$^1A_2''$	−0.7209	11.91	28	39			0.4440	K
												5	18			0.3390	K
$^3A_1''$	−0.7689	10.50	18	28			0.5766	K	($^1B_1$)	−0.6882	12.83	5	18			0.4440	K
			5	39			+0.2114					28	39			0.3430	K
($^3A_2$)	−0.7428	10.95$	5	39			0.5854	K		−0.6296	14.93	18	19	28	39	0.7089	S
			18	28			0.2189			−0.6204	14.79	4	18			0.3932	K
	−0.6691	14.09	5	18	19	39	0.4572	S				27	39			0.3681	K
			4	39			+0.1527										
	−0.6513	13.62	4	39			0.4977	K	$^1A_2'$	−0.7982	9.22	18	39			0.8247	K
			5	18	19	39	+0.2002			−0.6754	13.33	18	38			0.5154	S
	−0.6502	13.62†	18	27			0.6034	K	($^1B_2$)			18	38			0.1483	K
	−0.6491	13.59	5	18	19	39	0.7738	S				17	39			0.1438	K
										−0.6262	16.16	18	38			0.7631	K
$^3A_2''$	−0.7489	11.01$	5	18	28	39	0.7869	K				19	39			0.2416	S
	−0.7306	11.67	5	18	28	39	0.7850	K				17	39			0.1991	K
($^3B_1$)	−0.6729	13.03	27	39			0.3130	S/K		−0.5859	16.05	5	28			0.7959	K
			18	19	28	39	+0.3989										
	−0.6508	13.68†	4	18			0.6152	K									
	−0.6449	14.24	3	18			0.2849	S/K									
			18	19	28	39	+0.3395										
	−0.6325	14.24	27	39			0.4189	K/S									
			18	19	28	39	+0.3857										

[a] Degenerate levels are marked as follows: *, $1^3E'$; #, $2^3E'$; $, $1^3E''$; †, $2^3E''$. [b] CI sequence numbers (see Table III). [c] K = Koopmans'; S = shakeup; S/K or K/S = mixed. [d] Closed shell, 2 electrons in level 18. [e] Closed shell, 2 electrons in level 19.

numbers 5, 28) down to $1a_2''$ (16) in combination with 2e″ (18, 39) are found. These are clearly Koopmans'-type states and are expected to be relatively intense in the photoelectron spectrum. The following groups of states arise from the open-shell products:

$$E' \times E' = A_1' + A_2' + E'$$

$$E'' \times E'' = A_1'' + A_2'' + E''$$

$$E'' \times A_2'' = E'$$

$$E' \times A_2'' = E''$$

Examples of all types are found, but the operational requirement that S_3N_3 be treated in the lower point group of C_{2v} means that E′/E″ states do not automatically emerge. However, they are readily assigned (see Table V) on the basis of both almost exact degeneracy (0.05 eV) and composition of the configurations in the final state. A further general feature arising from the combinations of up to 6e in pairs of open-shell orbitals is that linear combinations of Koopmans'-type states occur. These do not always have simple internal ratios and can be quite widely spaced; for example, $(1e'')^3(2e'')^3$ yields $2^3A_1'$ and $3^3A_1'$ separated by 0.7 eV.

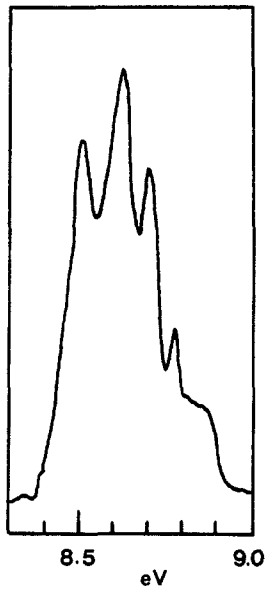

Figure 6. Expansion of the first ionization potential of S_3N_3.

The first IP (vertical, 8.62 eV) is calculated as $^3A_2'$ ($^3B_2$ in C_{2v}) corresponding to an unpaired $(2e'')^2$ configuration. The two singlets $^1A_1'$ ($^1A_1$ in C_{2v}, closed shell) and $^1A_2'$ ($^1B_2$ in C_{2v}, open shell) are computed some 1.2 and 0.9 eV, respectively, to higher binding energy. Given that only one distinct peak appears in the low IP region, it is feasible that the present calculations either under or overestimate the triplet–singlet splitting; inclusion of the MRDCI (unpublished results) does shift them around. The problem is that we cannot compute the intensities; it is, therefore, possible that weak features between 8.5 and 10 eV could conceal the singlet states.

Detailed analysis of the first IP (Figure 6) shows evidence for some vibrational structure, although no regular vibrational intervals are discernible; spacings of 630 and 870 ± 50 cm^{-1} can be measured. For a planar six-membered ring there are only two totally symmetric (A_1') modes, one involving symmetric stretching and the other a ring deformation. In $S_3N_3^-$ these modes are observed[34] at 700 and 590 cm^{-1}. We have seen, however, that it is quite feasible that the ground ionic state distorts through a Jahn–Teller mechanism to C_{2v}, thereby permitting observation of the nonsymmetric E′ modes, in this case, asymmetric stretching ring vibrations. In $S_3N_3^-$ these occur at 925 and 640 cm^{-1}. Given these four frequencies for the anion it is not possible to definitively assign modes for the ground-state cation. We do note that vaporization of $(SN)_x$ leads to a trapped red material having infrared frequencies at 996 and 634 cm^{-1} (matrix)[26] and 1045 and 680 cm^{-1} (trapped solid).[27] It is feasible that the observed species[26,27] is $S_3N_3^\circ$ (see also, discussion).

As mentioned above, the 11-eV band probably contains at least 3 IP's; the present calculations yield $^3A_1''$, $^3E''$, $^3A_2''$, $^3A_2'$ (low to high binding energy), as well as two shakeup peaks involving the HOMO → LUMO process. The singlet states $^1A_1''$, $^1A_2''$, and possibly $^1A_1''$ can also be accommodated under the 11-eV envelope (see Figure 5 for the correspondence of the triplet and singlet cationic states with a schematic experimental spectrum). The principal IP's of this group are all combinations of (4e′) × (2e″) as expected on the basis of Koopmans' theorem. The separation of the first two main bands of the PE spectrum (2.46 eV) is well reproduced by the present calculations, as is the smaller gap to the onset of the next band system. The third band centered around 12.9 eV exhibits 3 principal maxima and extends over nearly 2 eV. The present calculations obtain some 8 triplet and 10 singlet states in this region; many of these are shakeup states, of two main types $(i)^2(2e'')^3 \rightarrow (i)^1(2e'')^4$, where i is one of the group 4e′, 3e′, 1e″, and $(i)^2(2e'')^3 \rightarrow (i)^2(2e'')^2(3e'')^1$, i.e., HOMO → LUMO excitation. The principal triplet states in the low binding energy end near 12.5 eV are combinations of $(2e'')^1 \times (1e'')^1$, changing to $(2e'')^1 \times (3e')^1$ at the high binding energy end near 13.5 eV. The singlet manifold is shifted to the high end, with many more shakeup states being evident (Table V).

The fourth band at 14.2 eV is both weaker and sharper; the SCF calculations suggest that the innermost π level $1a_2''$ together with $3a_1'$ occur here. Although $3a_1'$ lies very close to $1a_2''$ in the SCF orbital sequence (Figure 4), we were unable to identify a Koopmans'-type state involving $3a_1'$ in the 8–15-eV range. This suggests that this orbital is not a dominant contributor to low-lying configurations.

Discussion and Conclusion

We have shown that under favorable experimental conditions, the vaporization of the $(SN)_x$ polymer yields a single species in the gas phase; this species is identified by means of a PE/PIMS combination as the previously unknown S_3N_3 radical. We find no evidence for a "quasilinear" $(SN)_4$ unit.[15–18] We should point out, however, that at a lower temperature (<130 °C) and with reduced pumping other species can be observed, predominantly S_2N_2, but also including S_4N_4 and S_4N_2. Such a mēlange, which can vary depending upon the conditions, has possibly led to confusion in earlier studies.[15–18,23,24] The same $S_3N_3^\circ$ species is also produced upon pyrolysis of S_4N_4 over glass or silver wool in agreement with earlier work.[29] In neither case is a 100% yield obtained; the balance is always S_2N_2, S_4N_4, and S_4N_2. In all three methods the products can be trapped at −196 °C and allowed, upon warming, to polymerize to $(SN)_x$. In the latter two cases, the main precursor to $(SN)_x$ is undoubtedly S_2N_2, as this is the well-known reaction by which most $(SN)_x$ is made.[5–7] We note that polymerization of S_2N_2 usually occurs in the presence of other "red" or "brown" materials[7] and that absolutely pure S_2N_2 (white) polymerizes extremely slowly (see ref 7 and the discussion that ensued).

"Pure" $S_3N_3^\circ$ condenses to form multicolored product(s), predominately red; from our observations this material is the most volatile, giving S_3N_3 and S_2N_2 back into the vapor phase upon warming from −196 °C (polymerization also occurs). It appears feasible, therefore, that S_3N_3 forms a red material upon condensation which can be revaporized or allowed to polymerize to $(SN)_x$. Although speculative it is also conceivable that this is the same material as observed by Love et al.[7] and identified by them as "red monomer". That species, also quite volatile, and also giving the polymer, was shown by EPR to be paramagnetic. It was claimed,[7] from mass spectrometric observations, to be monomeric NS. This is highly unlikely given the truly transient nature of NS, as determined from gas-phase electron resonance[46] and PE spectroscopy.[47] We do not see any PE evidence for the NS radical in our experiments, although we do note that the He I PIMS of S_3N_3 (Figure 2) shows a strong NS^+ (46 amu) mass peak. It is therefore quite reasonable that the electron impact ionization results on the red monomer[7] do indeed show a predominant NS^+ ion. A red material is, indeed, often seen in vaporization of $(SN)_x$ (see, e.g., ref 1, 24, 26, 27).

In short, it is conceivable that the "red monomer" of Love et al.[7] is S_3N_3. Whether or not this turns out to be the case does not prevent us from addressing the important question of how the $(SN)_x$ polymer with a chain structure and equal bond lengths can vaporize as a ring trimer. Equally, how does the trimer radical reform to give the polymer? The question is not without precedent, however, since square-planar S_2N_2 molecules can open to form the polymer, and as we have shown, the polymer can vaporize to yield square-planar S_2N_2. Although the mechanism of the latter has not been specifically tackled before, there is no doubt that polymerization of S_2N_2 occurs such as to give $(SN)_2$ units all within one chain, i.e., square-planar S_2N_2 opens up and adjacent units link together.[1,5–12] We would also mention that long-chain sulfur species may vaporize and form S_8, S_7, and S_6 rings.[48,49]

(46) Carrington, A.; Howard, B. J.; Levy, D. H.; Robertson, J. C. *Mol. Phys.* **1968**, *15*, 187–200.
(47) Dyke, J. M.; Morris, A.; Trickle, I. R. *J. Chem. Soc., Faraday Trans. 2* **1977**, *73*, 147–151.
(48) Berkowitz, J. In *Elemental Sulfur*; Meyer, B., Ed.; Interscience: New York, 1965.

Although a similar two-dimensonal mechanism involving only one chain is feasible for S_3N_3, we would prefer a three-dimensional approach. This is best envisaged for the vaporization step where two possibilities appear feasible. One would involve an SNS unit in the chain along the $\bar{1}02$ plane coupling to an NSN unit in the plane behind, i.e., coupling occurs approximately along the 100 plane. This produces the required six-membered ring with the central atom of the three from each chain flipped up. Such a process can continue down each pair of chains taking three atoms at a time from each. This process is facilitated by the close interaction between such units; S···N distances are 3.39 Å, close to the van der Waals radii (3.35 Å). The alternative mechanism is to take an NS fragment from one chain and insert it into a planar SNSN unit in the plane behind. This process would be considerably enhanced if one $(SN)_x$ chain were to rotate relative to the other. Such interchain coupling has already been shown to exist,[50-52] and from band structure calculations it is evident that this is a requirement for large π band splittings and the subsequent electrical properties of $(SN)_x$. Thus, although the individual chains can exhibit a one-dimensional Peierls instability (hence semiconducting) the three-dimensional solid exhibits metallic character. In both cases a distorted S_3N_3 ring will be produced initially, and it is therefore of some interest to determine the potential barrier for rearrangement to a planar structure. Such studies are at present underway; we have shown above that the chair/boat C_s symmetry $S_3N_3^{\circ}$ readily converts to the planar C_{2v} form. The reverse of either of the above mechanisms is a preferred topochemical polymerization, i.e., condensation of S_3N_3 units to $(SN)_x$ would require stacks of S_3N_3 ring units, not unlike those proposed for the S_2N_2 crystal structure.[6] Such cofacial π systems are currently the subject of some interest.[53] The "red monomer" can be obtained as an unstable crystalline solid;[7] the crystal structure would be of considerable interest in the context of the above discussion.

In closing, we reiterate that our ab initio CI calculations for the radical and cationic states support a planar ring geometry for the $S_3N_3^{\circ}$ species: essentially D_{3h} with a possible distortion to C_{2v}, and a shortening of the N–S–N bonds about the C_2 axis. The radical is $^2A_2$; the ground-state cation is $^3A_2'$, preferred over $^1A_1'$. This is analogous to the situation in the first-row NH_2 radical,[54] although this cation ordering is reversed in the second-row PH_2 species.[55] The agreement with the PES is remarkably good considering the complexity of ionic states.

Acknowledgment. We thank the Natural Sciences and Engineering Research Council of Canada for financial support. We thank Drs. McDowell and Frost (UBC) for their interest and Dr. M. F. Guest (Daresbury) for assistance with the MRDCI program.

Registry No. S_3N_3, 64885-69-4; $(SN)_x$, 56422-03-8; S_4N_4, 28950-34-7; NS_2, 12033-57-7; S_2N_2, 25474-92-4.

(49) Berkowitz, J.; Lifshitz, C. *J. Chem. Phys.* **1968**, *48* 4346–4350.
(50) Messmer, R. P.; Salahub, D. R. *Chem. Phys. Lett.* **1976**, *41*, 73–76.
(51) Berlinsky, A. J. *J. Phys. C* **1976**, *9*, L283–L284.
(52) Ching, W. Y.; Harrison, J. G.; Lin, C. C. *Phys. Rev. B* **1977**, *15*, 5975–5982.
(53) Boerē, R. T.; French, C. L.; Oakley, R. T.; Cordes, A. W.; Privett, J. A. J.; Craig, S. L.; Graham, J. B. *J. Am. Chem. Soc.* **1985**, *107*, 7710–7717.
(54) Dunlavey, S. J.; Dyke, J. M.; Jonathan, N.; Morris, A. *Mol. Phys.* **1980**, *39*, 1121–1135.
(55) Dyke, J. M.; Jonathan, N.; Morris, A. *Int. Rev. Phys. Chem.* **1982**, *2*, 3–42.
(56) Dyke, J. M.; Golob, L.; Jonathan, N.; Morris, A. *J. Chem. Soc., Faraday Trans. 2* **1975**, *71*, 1026–1036.
(57) Berkowitz, J. *J. Chem. Phys.* **1975**, *62*, 4074–4079.
(58) Boschi, R.; Schmidt, W. *Inorg. Nucl. Chem. Lett.* **1973**, *9*, 643–648.

Electrostatic Proximity Effects in the Relative Basicities and Acidities of Pyrazole, Imidazole, Pyridazine, and Pyrimidine[1]

Robert W. Taft,*† Frederick Anvia,† Mare Taagepera,† Javier Catalán,‡ and José Elguero§

Contribution from the Department of Chemistry, University of California at Irvine, Irvine, California 92717, the Departamento de Quimica Fisica y Quimica Cuantica, Universidad Autonoma de Madrid, Cantoblanco 28049, Madrid, Spain, and the Instituto de Quimica Medica, CSIC, Juan de la Cierva 3, 28006, Madrid, Spain. *Received August 30, 1985*

Abstract: The relative gas-phase and solution basicities of pyridazine and pyrimidine and of pyrazole and imidazole, as well as the relative gas-phase and solution acidities of the latter diazoles, have been accounted for approximately by considering important NH^+ and lone pair electrostatic interactions that act from the 2-position.

The acid/base behavior of above titled compounds is widely recognized for its importance to the life sciences.[2] The gas- and aqueous-phase basicities of pyrimidine (1,3-diazine, I) are known to be distinctly *smaller* by 3.4[3] and 1.1[4] pK_b units, respectively, than that of pyridazine (1,2-diazine, II). We have found that *in contrast* the gas-phase basicity of imidazole (1,3-diazole, III) is *larger* (as is also the aqueous basicity[5]) by significantly greater amounts (8.0 and 4.6 pK_b units, respectively) than that of pyrazole (1,2-diazole, IV). This very large basicity difference (in either phase) has not previously been satisfactorily explained.

We have also found that the gas-phase basicity of the conjugate base of imidazole (III′) is significantly *smaller* (by 2.6 pK_b units) than that of the conjugate base of pyrazole (IV′). That is, III is a stronger acid than IV. The same order of relative acidities applies in dimethyl sulfoxide solution (III is stronger than IV by

† University of California at Irvine.
‡ Universidad Autonoma de Madrid.
§ Instituto de Quimica Medica.

(1) This work was supported in part by a grant from the U.S.-Spain Joint Committee for Scientific and Technological Cooperation.
(2) (a) Schofield, K. S.; Grimmett, M. R.; Keene, B. R. T., *The Azoles*; Cambridge University Press: Cambridge, **1976**; p 23. (b) *Comprehensive Heterocyclic Chemistry*; Katritzky, A. R., Rees, C. W., Eds.; Pergamon: Oxford, **1984**; Vol. 5, p 49.
(3) Houriet, R.; Schwarz, H.; Zummack, W.; Androde, J. G.; Schleyer, P. v. R. *Nouv. J. Chim.* **1981**, *5*, 505. The value given is from our determinations, which are in reasonable accord with this reference. We find the gas-phase basicity of II to be equal (±0.1 kcal/mol) to that of ethylamine and to be 1.1 kcal/mol (±0.1) greater than that of 3-chloropyridine. Compound I was found to be 1.4 ± 0.2 kcal/mol more basic than 4-CNC_5H_4N, all using the methods described in ref 14. Gas-phase $\Delta pK_b = \Delta G^{\circ}(g)/2.303RT$, where ΔG° is for the indicated proton-transfer equilibrium.
(4) Kasende, O.; Zeegers-Huyskens, Th. *J. Phys. Chem.* **1984**, *88*, 2132. This paper reports the same order of hydrogen-bond basicity properties.

0002-7863/86/1508-3237$01.50/0 © 1986 American Chemical Society